Closed-Form BER Expression for OFDM with the Effect of TI-ADC's Timing Mismatch

Vo-Trung-Dung Huynh, Nele Noels, Heidi Steendam
Department of Telecommunications and Information Processing, Ghent University
{votrungdung.huynh, nele.noels, heidi.steendam}@ugent.be

***Abstract*—Timing mismatch in time-interleaved analog-to-digital converters (TI-ADCs) may cause a significant performance degradation in high-speed orthogonal frequency division multiplexing (OFDM) systems. To evaluate the impact of this impairment in such systems, we first derive a mathematical expression for the output of the discrete Fourier transform (DFT) unit that is used to demodulate the received OFDM signal samples. From the obtained expression, it follows that a TI-ADC with timing mismatch causes a phase rotation of the desired symbols and generates inter-carrier interference (ICI). Building on this result, we further derive an approximate closed-form bit error rate (BER) expression for quadrature amplitude modulation (QAM) or pulse amplitude modulation (PAM), assuming an additive white Gaussian noise (AWGN) channel and binary reflected Gray code (BRGC) mapping. Numerical results are provided to demonstrate the accuracy of the presented formula.**

***Index Terms*—Bit error rate, OFDM, time-interleaved analog-to-digital converter, timing mismatch, PAM, QAM.**

I. Introduction

Orthogonal frequency division multiplexing (OFDM) is used in many wired and wireless broadband communication systems thanks to its high spectral efficiency and tolerance against channel dispersion [1]. The use of OFDM in multi-Gigabit fiber-optic communication systems, in which data rates are extremely high, has recently attracted increasing interest (see [2] and the references therein). For example, the transmission of 132.2 Gbit/s within an optical bandwidth of 25 GHz was studied in [3]. At these very high data rates, OFDM systems require a high sampling rate analog-to-digital converter (ADC) placed prior to the baseband digital signal processing unit at the receiver. Because the sampling rates of regular ADCs are limited by the physical constraints of the current technology [4], a time-interleaved (TI) structure of L identical parallel ADCs is often used as a practical alternative. To achieve a sampling rate $\frac{1}{T_s}$ in a TI-ADC, L sub-ADCs each sample the analog input signal at a lower rate $\frac{1}{LT_s}$, i.e., the l-th sub-ADC samples the input signal at timing instants $t_k^{(l)} = kLT_s + lT_s$, where $k = 0, 1, 2, ...$ and $l = 0, 1, ..., L-1$. Unfortunately, mismatches between the parallel sub-ADCs of a TI-ADC, such as offset, gain and timing mismatch, can significantly degrade the performance of a TI-ADC-based communication system. The effects of TI-ADC's mismatches on the system performance were studied for single-carrier systems in [5-7], and for multi-carrier systems in [8-9]. Moreover, closed-form bit error rate (BER) expressions were derived for OFDM systems impaired by a TI-ADC's offset mismatch [10] and a TI-ADC's gain mismatch [11]. Those closed-form expressions allow efficient and fast evaluation of the BER performance, in particular when compared to time-consuming Monte-Carlo computations [8]. However, to the best of our knowledge, a closed-form BER expression for OFDM systems revealing the effect of a TI-ADC's timing mismatch has not been derived yet. In this paper, we analytically derive such a BER expression based on a Gaussian approximation of the inter-carrier interference caused by the timing mismatch. To isolate the effect of the timing mismatch, an additive white Gaussian noise (AWGN) channel is considered. Further, we assume quadrature amplitude modulation (QAM) and bit-to-symbol mapping based on the binary reflected Gray code (BRGC) [12]. The accuracy of the derived BER expression will be assessed by comparing the theoretical results with empirical Monte-Carlo simulations.

The paper is organized as follows. Section II describes the considered system model, and details the derivation of discrete Fourier transform (DFT) output expression to quantify the phase rotation and the inter-carrier interference (ICI) caused by the timing mismatch. From the DFT output formula, we are able to derive the BER expression for a rectangular QAM constellation in Section III. The BER expressions for square QAM and pulse amplitude modulation (PAM) constellations are presented as special cases. In Section IV, we illustrate the phase rotation and the ICI on scatter diagram and validate the accuracy of the derived BER expression. Conclusions are provided in Section V.

II. System Description

Fig. 1 illustrates the block diagram of the considered OFDM system. To simplify the notations, we consider the transmission of a single OFDM symbol only. The discrete baseband OFDM signal is given by:

$$s_k = \frac{1}{\sqrt{N}} \sum_{a=0}^{N-1} X_a e^{j2\pi \frac{ak}{N}}, \qquad k = 0, 1, ..., N-1, \qquad (1)$$

where N denotes the number of sub-carriers in the OFDM system. Further, in (1), $X_a \neq 0$, if $a \in I_d$ and $X_a = 0$, if $a \notin I_d$, where $I_d = \{N/2 - N_d/2, ..., N/2 + N_d/2 - 1\}$ with $N_d < N$ the number of data-modulated sub-carriers[1].

[1]In practice, in many OFDM systems, not all N sub-carriers are used for data transmission. For instance, a few sub-carriers near the edges (i.e., the guard band) are not modulated to achieve a sufficient transition band at the bandwidth boundaries [13].

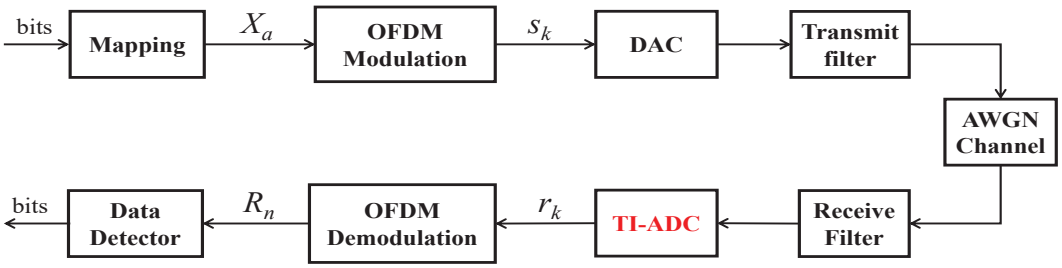

Fig. 1. Block diagram of an OFDM system with a TI-ADC at the receiver.

Moreover, the data symbols $X_a \neq 0$ are taken from a unit-energy rectangular $M_I \times M_Q$-QAM constellation, in which $(\log_2 M_I + \log_2 M_Q)$ bits are mapped on the constellation points. Before transmission over an AWGN channel with noise power spectral density N_0, the OFDM signal passes through a digital-to-analog converter (DAC) and a transmit filter.

At the receiver, assuming perfect matched filtering, the resulting waveform is sampled at Nyquist rate $\frac{1}{T_s}$ by a TI-ADC consisting of L parallel sub-ADCs. The l-th sub-ADC samples the input signal at time instants $kLT_s + lT_s + dt_l T_s$, where $k = 0, 1, ..., N-1$, $l = 0, 1, ..., L-1$ and dt_l denotes the relative timing mismatch value of the l-th sub-ADC. The TI-ADC is assumed to have a sufficiently high resolution such that the quantization noise can be neglected [14]. In practice, the timing mismatch values $dt_l T_s$ of the sub-ADCs in a TI-ADC vary slowly [9], and therefore we model them as constants over the duration of an OFDM symbol. Using the model from [7], the output of the TI-ADC with timing mismatch can be expressed by:

$$r_k = \sum_{l=0}^{L-1} \sum_{q=-\infty}^{+\infty} \left(\sqrt{E_s} s_k(dt_l) + w_k\right) \cdot \delta_{k-qL-l}, \quad k = 0, 1, ..., N-1, \tag{2}$$

where r_k denotes the k-th received sample, E_s is the transmitted symbol energy, δ_k denotes the Kronecker delta, w_k are independently and identically distributed (i.i.d.) AWGN noise samples with zero mean and variance $\sigma_w^2 = \frac{N_0}{2}$ per dimension, and $s_k(dt_l)$ is defined as:

$$s_k(dt_l) = \frac{1}{\sqrt{N}} \sum_{a=0}^{N-1} X_a e^{j2\pi \frac{a(k-dt_l)}{N}}. \tag{3}$$

The samples r_k (2) are applied to a size-N discrete Fourier transform (DFT) unit. The DFT output is given by:

$$\begin{aligned} R_n &= \tfrac{1}{\sqrt{N}} \sum_{k=0}^{N-1} r_k e^{-j2\pi \frac{kn}{N}} \\ &= \sqrt{E_s} DT_{0,n} X_n + \Phi_n, \qquad n = 0, 1, ..., N-1, \end{aligned} \tag{4}$$

where X_n are the transmitted symbols. Further, the interference-plus-noise term Φ_n in (4) decomposes as:

$$\Phi_n = \Phi_{1,n} + W_n, \tag{5}$$

where W_n are i.i.d. Gaussian random variables with zero mean and variance $\sigma_w^2 = \frac{N_0}{2}$ per dimension, and $\Phi_{1,n}$ is the ICI term caused by the timing mismatch, given by:

$$\Phi_{1,n} = \sqrt{E_s} \sum_{i=1}^{L-1} \sum_{a=0}^{N-1} DT_{i,a} X_a f(a - p_i) e^{-j\pi(a-p_i)}, \tag{6}$$

with

$$DT_{x,z} = \frac{1}{L} \sum_{l=0}^{L-1} e^{-j2\pi \frac{xl}{L}} e^{-j2\pi \frac{z dt_l}{N}}, \tag{7}$$

$$f(z) = \begin{cases} \frac{\sin(\pi z)}{\pi z} & , \text{if } N/L \text{ is non} - \text{integer} \\ \delta(z) & , \text{if } N/L \text{ is integer} \end{cases} \tag{8}$$

and $p = \mathrm{mod}\left(n - i\frac{N}{L}, N\right)$ denoting the remainder after division of $n - i\frac{N}{L}$ by N. Note that in the case of integer ratios $\frac{N}{L}$, $\Phi_{1,n} = \sum_{i=1}^{L-1} DT_{i,p} X_p$. The quantities R_n from (4) are used to perform bit sequence detection by mapping them to the nearest constellation point and applying the inverse mapping rule.

Let us now take a closer look at the factor $DT_{0,n}$ in (4). Using a Taylor series expansion for the exponential function and making a first order approximation, $DT_{0,n}$ can be written as:

$$\begin{aligned} DT_{0,n} &= \tfrac{1}{L} \sum_{l=0}^{L-1} e^{-j2\pi \frac{n dt_l}{N}} \\ &\approx e^{-j2\pi \frac{n}{N} \cdot \frac{1}{L} \sum_{l=0}^{L-1} dt_l}. \end{aligned} \tag{9}$$

From (4) and (9), it follows that the timing mismatch causes a phase rotation of the desired symbols. The magnitude of this rotation angle linearly depends on the sub-carrier index and the average of the timing mismatch values, i.e., $\frac{1}{L}\sum_{l=0}^{L-1} dt_l$.

III. BER Analysis

In order to determine the effect of TI-ADC's timing mismatch on the BER performance, we first consider the interference-plus-noise term Φ_n (5). Assuming that the transmitted data symbols X_n can be modelled as statistically independent random data symbols that are uniformly distributed over a unit-energy constellation, it immediately follows that:

1) $\Phi_{1,n}$ and W_n are statistically independent with zero mean.
2) Because dt_l is constant, $DT_{x,z}$ (7) is deterministic. As a result, $\Phi_{1,n}$ (6) is the weighted sum of independent random variables. Hence, taking into account the weighted central limit theorem [15], $\Phi_{1,n}$ can be considered as a Gaussian distributed variable for the case of non-integer ratios $\frac{N}{L}$, if N or L is sufficiently large, and for the case of integer ratios $\frac{N}{L}$, if L is sufficiently large. The variance $\sigma^2_{\Phi^{\beta}_{1,n}}$ of $\Phi_{1,n}$ in the β-dimension is given by:

$$\sigma^2_{\Phi^{\beta}_{1,n}} = \begin{cases} \Re\{\Psi\}, \text{if } \beta = I \\ \Im\{\Psi\}, \text{if } \beta = Q \end{cases}, \tag{10}$$

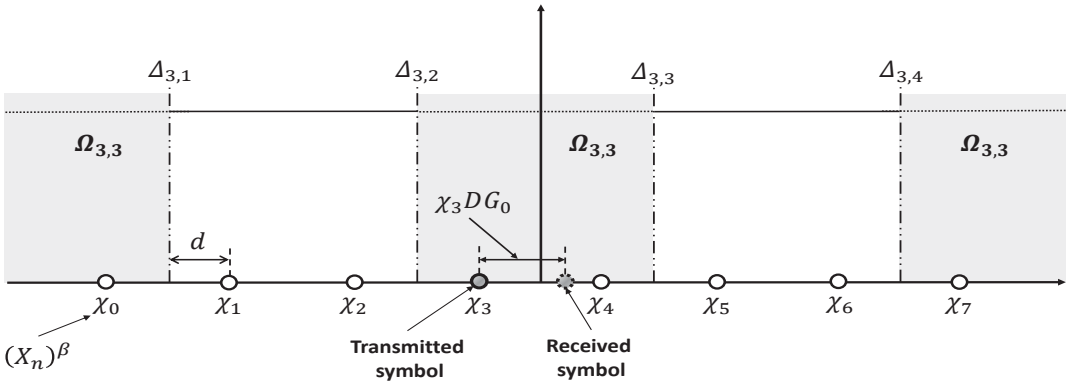

Fig. 2. An illustration of the decision regions and boundaries required to derive the BER expression for $M_\beta = 8, u = 3, v_\beta = 3$.

where $\beta \in \{I, Q\}$ refers to the in-phase (I) and quadrature (Q) dimensions of the symbol, $\Re\{z\}$ and $\Im\{z\}$ denote the real and imaginary part of z, respectively. Further, $\Psi_{i_1,i_2,a}$ in (10) is defined as:

$$\Psi = E_s \sum_{i_1=1}^{L-1} \sum_{i_2=1}^{L-1} \sum_{a=0}^{N-1} DT_{i_1,a} (DT_{i_2,a})^* (\xi + j(1-\xi)) \times f(a - p_{i_1}) f(a - p_{i_2}) e^{-j\pi(p_{i_2} - p_{i_1})}, \tag{11}$$

where ξ is the average energy per symbol in the I dimension of the constellation[2], and $(z)^*$ denotes the complex conjugate of the complex-valued variable z.

3) W_n is Gaussian distributed with variance $\sigma_w^2 = \frac{N_0}{2}$ per dimension.

In conclusion, for non-integer ratios $\frac{N}{L}$, if N or L is large, and for integer ratios $\frac{N}{L}$, if L is large, the interference-plus-noise term Φ_n (5) can be approximated as a complex-valued Gaussian random variable with independent real and imaginary components, having zero mean and variance $\sigma^2_{\beta,n}$ in the β-dimension given by:

$$\sigma^2_{\beta,n} = \sigma^2_{\Phi^\beta_{1,n}} + \sigma^2_w. \tag{12}$$

Let us now denote the rectangular QAM constellation symbols X_n as $\chi_{v_I} + j\chi_{v_Q}$, with

$$\chi_{v_\beta} = (2v_\beta + 1 - M_\beta) d_\beta, \tag{13}$$

where $v_\beta \in \{0, 1, ..., M_\beta - 1\}$ and d_β denotes the half minimum Euclidean distance in the β-dimension. Further, for the BRGC mapping rule, we denote the m_β bit sequence that corresponds to χ_{v_β} as $\hat{\mathbf{b}}^{(v_\beta)} = \left(\hat{b}_1^{(v_\beta)}, \hat{b}_2^{(v_\beta)}, ..., \hat{b}_{m_\beta}^{(v_\beta)}\right)$:

$$\chi_{v_\beta} \leftrightarrow \hat{\mathbf{b}}^{(v_\beta)} = (v_\beta)_2 \oplus \left(\left\lfloor \frac{v_\beta}{2} \right\rfloor\right)_2, \tag{14}$$

where $(z)_2$ denotes the natural binary code of integer z and $\lfloor z \rfloor$ denotes the largest integer smaller than z. To derive the BER expression, we follow the procedure outlined in [11]. It follows that the BER with the effect of the timing mismatch on a rectangular QAM constellation can be computed as:

$$BER = \frac{1}{2N_d M_I M_Q (m_I + m_Q)} \cdot \sum_{\beta,n,u,v_I,v_Q} \left(\sum_{y=1}^{F_{u,v_\beta}} \lambda_{u,v_\beta,y} erfc\left(\Gamma^\beta_{n,u,v_I,v_Q,y}\right) + \sum_{y=F_{u,v_\beta}+1}^{2^{u-1}} \mu_{u,v_\beta,y} erfc\left(-\Gamma^\beta_{n,u,v_I,v_Q,y}\right) \right), \tag{15}$$

where $\beta \in \{I, Q\}$, $m_\beta = \log_2 M_\beta$, $n \in N_d$, $u \in \{1, 2, ..., m_\beta\}$ and $v_\beta \in \{0, 1, ..., M_\beta - 1\}$. In (15), F_{u,v_β} indicates the number of decision region boundaries left of the considered constellation point. For binary reflected Gray code (BRGC) mapping [12], we have

$$F_{u,v_\beta} = \left\lfloor (2v_\beta + 1) \cdot 2^{-(m_\beta - u + 2)} + 2^{-1} \right\rfloor. \tag{16}$$

Further, in (15), $erfc(.)$ is the complementary error function (erfc-function): $erfc(x) = \frac{2}{\sqrt{\pi}} \int_x^\infty e^{-z^2} dz$, and the argument $\Gamma^\beta_{n,u,v_I,v_Q,y}$ of the erfc-function is defined as:

$$\Gamma^\beta_{n,u,v_I,v_Q,y} = \left(\left(DT_{0,n}\left(\chi_{v_I} + j\chi_{v_Q}\right)\right)^\beta - \Delta^\beta_{u,y} \right) \sqrt{\frac{E_s}{2\sigma^2_{\beta,n}}}, \tag{17}$$

where $(z)^\beta$ is defined as:

$$(z)^\beta = \begin{cases} \Re\{z\} & \text{, if } \beta = I \\ \Im\{z\} & \text{, if } \beta = Q \end{cases}, \tag{18}$$

and $\Delta_{u,y}$ is the y-th boundary (from left to right) on the decision region Ω_{u,v_β}[3] [16] (see an example in Fig. 2):

$$\Delta^\beta_{u,y} = \left((2y-1) \cdot 2^{m_\beta - u + 1} - M_\beta\right) d_\beta. \tag{19}$$

Finally, the pre-factors $\lambda_{u,v_\beta,y}$ and $\mu_{u,v_\beta,y}$ in (15) take the values $+1$ or -1 according to:

$$\lambda_{u,v_\beta,y} = (-1)^{\left\lfloor 2^{u-2-m_\beta} \cdot \left(\left(\chi_{v_\beta} - \Delta_{u,y}\right)/d_\beta - 1 \right) \right\rfloor} \tag{20}$$

and

$$\mu_{u,v_\beta,y} = (-1)^{\left\lfloor 2^{u-2-m_\beta} \cdot \left(-\left(\chi_{v_\beta} - \Delta_{u,y}\right)/d_\beta - 1 \right) \right\rfloor} \tag{21}$$

[2]Since the constellation was considered to have unit-energy, the average energy per symbol in the Q dimension of the constellation is then $1 - \xi$.

[3]Ω_{u,v_β} indicates the union of intervals of $\frac{1}{\sqrt{E_s}}(R_n)^\beta$ from (4), for which the received bit is decided to equal the transmitted bit.

The corresponding BER expression for an M_s-ary square QAM constellation is obtained by setting $M_I = M_Q = \sqrt{M_s}$ and $d_I = d_Q$. Similarly, the BER expression for an M_p-ary PAM constellation is derived by setting $M_I = M_p$, $M_Q = 1$; the sum over the Q dimension disappears. The expression (15) allows us to efficiently evaluate the BER performance of OFDM systems impaired by a TI-ADC's timing mismatch, avoiding the need for an extensive Monte-Carlo simulation, which is very time consuming.

IV. Numerical Results

In this section, we first observe the scatter diagram of the signal contribution to the DFT output samples to illustrate the influence of the phase rotation and the ICI caused by a timing mismatch. Then, we validate the accuracy of the derived BER expression by comparing the theoretical results with Monte-Carlo simulations for different constellations and mismatch levels. Finally, we investigate the influence of the DFT size N and the number L of sub-ADCs on the correctness of the proposed BER expression. We assume all sub-carriers are modulated, i.e., $N_d = N$, and the sampling time T_s and the transmitted symbol energy E_s are normalized, i.e., $T_s = E_s = 1$. We generate $L = 320$ independent relative timing mismatch values[4] $dt_l^{(100\%)}$ according to a uniform distribution over the interval $[-1, 1]$ [9] and keep these fixed over the simulations. These L values can be interpreted as 100% of the timing mismatch level of a particular TI-ADC realization. Further, when $L = x < 320$, only the first x values of the 320 fixed relative timing mismatch values will be employed. Moreover, the level of timing mismatch will be varied by scaling the $dt_l^{(100\%)}$ timing mismatch values, i.e., for a $z\%$ mismatch level, we use as the timing mismatch values: $dt_l^{(z\%)} = \frac{z}{100} dt_l^{(100\%)}$.

Fig. 3 shows the combined effects of rotation and ICI in R_n (blue markers) from (4) in the absence of noise, i.e., $W_n = 0$. Further, Fig. 3 also illustrates the rotation effect separately, i.e., $DT_{0,n}X_n$ (yellow markers). As expected, we observe in Fig. 3 that the magnitude of the rotation angle increases and the ICI becomes more severe when the mismatch level increases. Further, Fig. 3 also reveals that the ICI dominates over the rotation effect.

In Fig. 4, the BER curves are shown for different mismatch levels, modulation types and orders. For comparison, the BER curves for the same systems without mismatch are also provided. Further, we assume $N = 2048$ and $L = 320$. We make the following observations:

1) Mismatch versus no mismatch: Fig. 4 obviously shows that the timing mismatch causes a system performance degradation, which is more severe as either the mismatch level or the modulation order increases.
2) Theory versus simulation: It is evident from Fig. 4 that the analytical BER curves are in excellent agreement with the simulated BER curves. We also investigated numerous other parameter settings (results are not shown in this paper), and found similar results as long as N and L are sufficiently large. This demonstrates the accuracy of the proposed BER expressions.

[4]This L is equal to the number of sub-ADCs in the 56 Gsa/s 8-bit TI-ADC in 65 nm CMOS technology designed by Fujitsu for 100 Gbps communication systems [17].

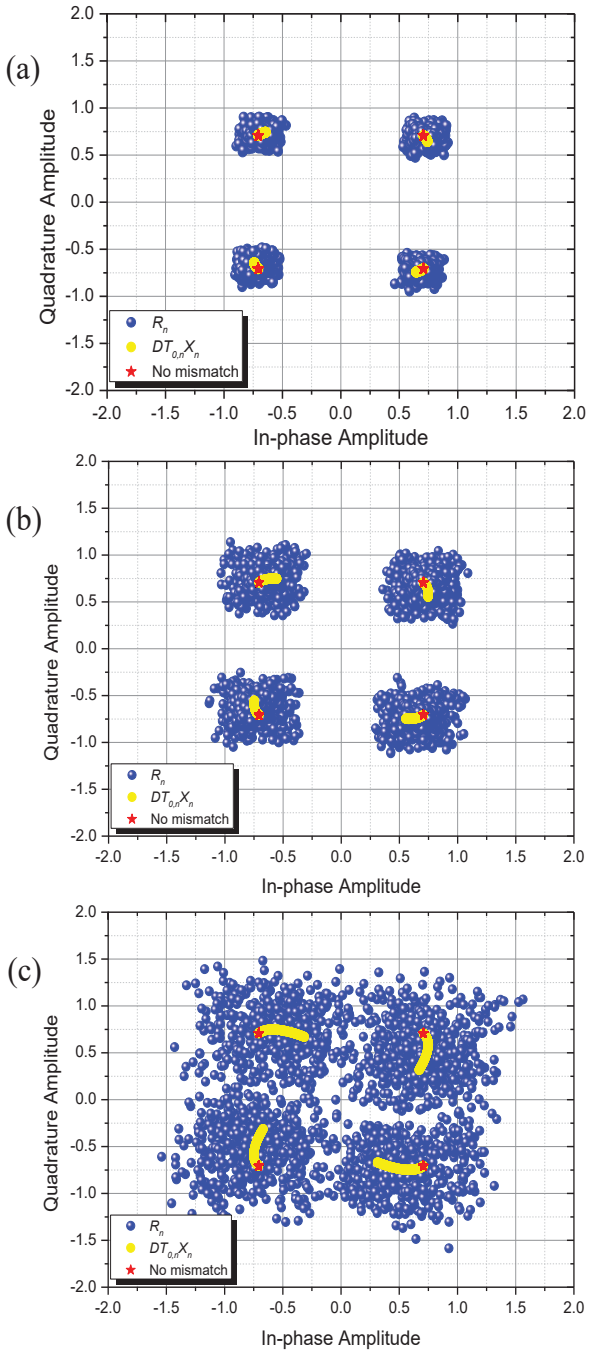

Fig. 3. Scatter diagram of the received 4-QAM symbols without noise for $N = 2048$ and $L = 8$: (a) 5% mismatch; (b) 10% mismatch and (c) 20% mismatch.

Fig. 5 shows the empirical and theoretical BER results for 16 QAM, 5% mismatch, and different values of N and L. We make the following observations:

1) Integer ratios $\frac{N}{L}$: Fig. 5(a) with $N = 2048$ shows that the analytical BER curves do not match the simulated BER curves when L is low, i.e., $L = 2, 32$. However, when L increases, the deviation between theory and

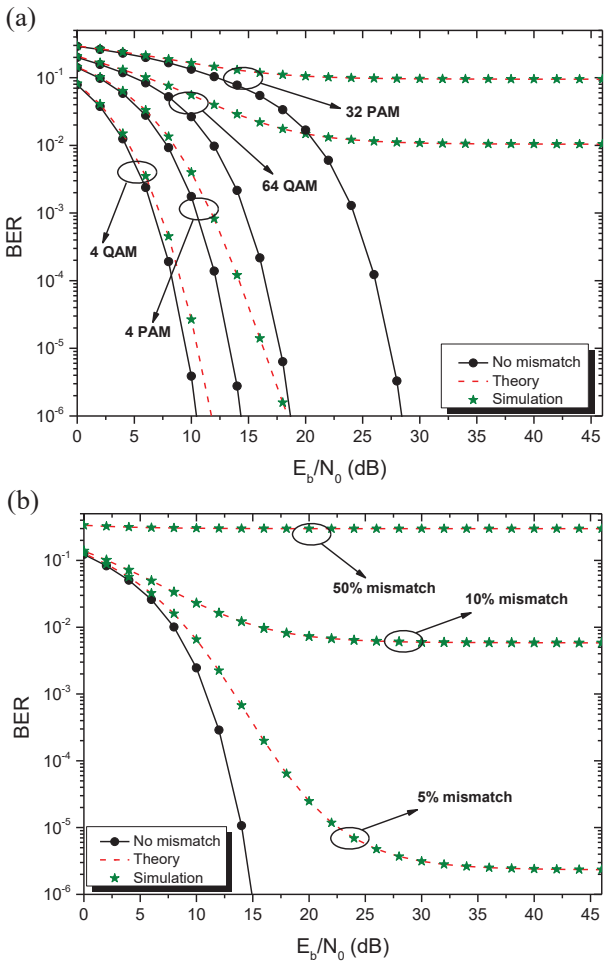

Fig. 4. BER curves with $N = 2048$ and $L = 320$: (a) 5% mismatch, square QAM and PAM; (b) 4×2 QAM, 5%, 10% and 50%.

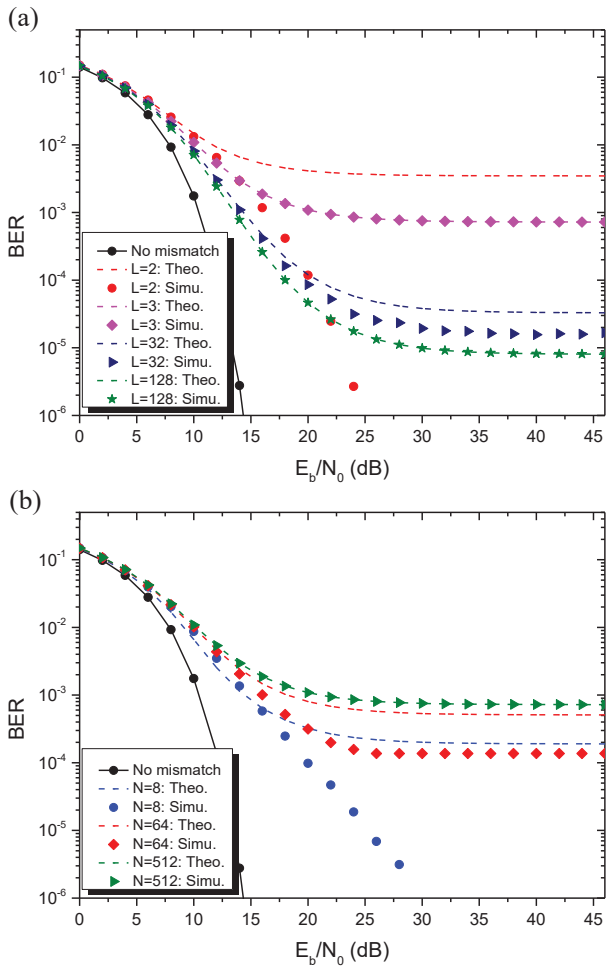

Fig. 5. BER curves for 16 QAM and 5% mismatch: (a) $N = 2048$ and $L = 2, 3, 32, 128$; (b) $L = 3$ and $N = 8, 64, 512$.

simulation decreases. When L equals 128, the theoretical results are in good agreement with the simulations. The deviation between theoretical results and simulations can be explained as follows. With integer ratios $\frac{N}{L}$, $\Phi_n = \sum_{i=1}^{L-1} DT_{i,p}X_p + W_n$, i.e., the sum only contains L terms. Hence, when L is small, Φ_n cannot be approximated as a Gaussian random variable because the weighted central limit theorem does not hold. Further, Fig. 5(a) illustrates that when L increases, the performance degradation decreases. This performance degradation depends on the relative timing mismatch values dt_l. Hence, the degradation will be different if we select another set of mismatch values dt_l.

2) Non-integer ratios $\frac{N}{L}$, small L and large N: From Fig. 5(a) with $N = 2048$, it follows that the theoretical BER curves are in good agreement with the simulated BER curves when $L = 3$. This can be explained as follows. With non-integer ratios $\frac{N}{L}$, the contribution of the timing mismatch is spread over all sub-carriers. This is in contrast to the case of integer ratios $\frac{N}{L}$, where the sum over N disappears. Therefore, $\Phi_{1,n}$ (6) consists of a sum over a large number N of terms, implying that it can be approximated as a Gaussian random variable when N is sufficiently large. Consequently, also Φ_n (5) behaves as a Gaussian random variable.

3) Non-integer ratios $\frac{N}{L}$, small L and small N: Fig. 5(b) with $L = 3$ reveals that the theoretical BER curves do not match the simulations when $N = 8, 64$, i.e., the Gaussian approximation no longer holds. The deviation between theory and simulation reduces as N increases. For $N = 512$, the theoretical BER curve matches well the simulated BER curve.

It should be noticed that 1) the high-speed OFDM systems that are usually employed for broadband applications typically have thousands of active sub-carriers [1] and 2) in the coming years, the number of sub-ADCs in TI-ADC architectures will further increase to obtain extremely high sampling rates. Under these circumstances, the approximate BER expression derived in this paper is a useful tool to evaluate the BER performance in practice. Finally, we would like to point out that even when the obtained BER is less accurate for the case of integer ratios $\frac{N}{L}$ and small L, or for the case of non-integer ratios $\frac{N}{L}$, small L and N, the derived BER expression can still serve as a useful upper bound on the true BER.

V. Conclusions

In this paper, we investigated the phase rotation and the ICI caused by a TI-ADC's timing mismatch in an OFDM system. The results show that the ICI effect dominates over the phase rotation effect. Further, we also derived an approximate closed-form BER expression for PAM and QAM-OFDM systems impaired by a TI-ADC's timing mismatch in a AWGN channel. The theoretical BER analysis is compared with the simulations, and the results show a very good agreement between theory and simulation when either the DFT size N or the number L of sub-ADCs is sufficiently large.

Acknowledgment

This research has been funded by the Interuniversity Attraction Poles Programme initiated by the Belgian Science Policy Office. The authors acknowledge the financial support from the Flemish fund for Scientific Research (FWO).

References

[1] R. V. Nee and R. Prasad, *OFDM for Wireless Multimedia Communications*, Boston, MA: Artech House, 2000.

[2] J. Armstrong, "OFDM for Optical Communications," *J. Lightwave Technol.*, vol. 27, no. 1, pp. 189-204, Feb. 2009.

[3] S. L. Jansen, A. A. Amin, H. Takahashi, I. Morita and H. Tanaka, "132.2 Gb/s PDM-8QAM-OFDM Transmission at 4-b/s/Hz Spectral Efficiency," *Photonics Tech. Lett.*, vol. 21, no. 12, pp. 802-804, Jun. 2009.

[4] W. C. Black and D. A. Hodges, "Time Interleaved Converter Arrays," *IEEE J. Solid-State Circuits*, vol. SSC-15, no. 6, pp. 1022-1029, Dec. 1980.

[5] A. Petraglia and S. K. Mitra, "Analysis of Mismatch Effects Among A/D Converters in a Time-Interleaved Waveform Digitizer," *IEEE Trans. Inst. Meas.* , vol. 40, no. 5, pp. 831-835, Oct. 1991.

[6] J. Elbornsson, F. Gustafsson, and J-E. Eklund, "Analysis of Mismatch Effects in a Randomly Interleaved A/D Converter System," *IEEE Trans. on Circuits and Systems*, vol. 52, no. 3, pp. 465-476, Mar. 2005.

[7] C. Vogel, "The Impact of Combined Channel Mismatch Effects in Time-Interleaved ADCs," *IEEE Trans. Instrum. Meas.*, vol. 54, no. 1, pp. 415-427, Feb. 2005.

[8] V.-T.-D. Huynh, N. Noels, P. Rombouts, J. Armstrong, and H. Steendam, "Effect of Time-Interleaved Analog-to-Digital Converter Mismatches on OFDM Performance," *IEEE Inter. OFDM Workshop*, Essen, Germany, Aug. 2014.

[9] S. Ponnuru, M. Seo, U. Madhow and M. Rodwell, "Joint Mismatch and Channel Compensation for High-Speed OFDM Receivers with Time-Interleaved ADCs," *IEEE Trans. Comm.*, vol. 58, no. 8, pp. 2391-2401, Aug. 2010.

[10] V.-T.-D. Huynh, N. Noels and H. Steendam, "Effect of Offset Mismatch in Time-Interleaved ADC Circuits on OFDM-BER performance," *IEEE Trans. Circuits Syst.*, pp. 2195 - 2206, vol. 64, no. 8, Aug. 2017.

[11] V.-T.-D. Huynh, N. Noels and H. Steendam, "Approximate Bit Error Rate for High-Speed OFDM Systems Impaired by a Gain Mismatch of a TI-ADC Realization," 24^{th} *Inter. Conf. Telecomm.*, Limassol, Cyprus, May 2017.

[12] M. Gardner, *Knotted Doughnuts and Other Mathematical Entertainments*, W.H. Freeman & Company, 1986 .

[13] I. Guvenc, S. Gezici, Z. Sahinoglu and U. C. Kozat, *Reliable Communications for Short-range Wireless Systems*, Cambridge University Press, USA, 2011.

[14] H. Johansson and P. Lowenborg, "Reconstruction of Non-Uniformly Sampled Bandlimited Signals by Means of Digital fractional Delay Filters," *IEEE Trans. Signal Proc.*, vol. 50, no. 11, pp. 2757-2767, Nov. 2002.

[15] M. Weber, "A Weighted Central Limit Theorem," *Statistics and Probability Lett.*, vol. 76, no. 14, pp. 1482-1487, Aug. 2006.

[16] P. K. Vitthaladevuni and M. S. Alouini, "A Closed-Form Expression for The Exact BER of Generalized PAM and QAM Constellations," *IEEE Trans. Comm.*, vol. 52, no. 5, pp. 698-700, May 2004.

[17] P. Bower, I. Dedic, "High speed converters and DSP for 100G and beyond," *Opt. Fiber Technol.*, vol. 17, no. 5, pp. 464-471, Oct. 2011.